DALTON
FULL PAPER

Cubane shaped clusters, precursors for aluminophosphate frameworks: a solid state multinuclear NMR study, in time and frequency domains

Thierry Azaïs,[a] Christian Bonhomme,*[a] Laure Bonhomme-Coury,[b] Jacqueline Vaissermann,[c] Yannick Millot,[d] Pascal P. Man,[d] Philippe Bertani,[e] Jérôme Hirschinger[e] and Jacques Livage[a]

[a] *Laboratoire Chimie de la Matière Condensée, Université P. et M. Curie, 4 Place Jussieu, 75252 Paris Cedex 05, France. E-mail: bonhomme@ccr.jussieu.fr*
[b] *Laboratoire Céramiques et Matériaux Minéraux, Ecole Supérieure de Physique et Chimie Industrielles de la Ville de Paris, 10 rue Vauquelin, 75231 Paris Cedex 05, France*
[c] *Laboratoire de Chimie des Métaux de Transition, Université P. et M. Curie, 4 Place Jussieu, 75252 Paris Cedex 05, France*
[d] *Laboratoire de Chimie des Surfaces, Université P. et M. Curie, 4 Place Jussieu, 75252 Paris Cedex 05, France*
[e] *Institut de Chimie, UMR 50 CNRS, Université Louis Pasteur, 67008 Strasbourg, France*

Received 31st May 2001, Accepted 17th December 2001
First published as an Advance Article on the web 29th January 2002

A detailed solid state NMR study of molecular aluminophosphates is presented. The crystallographic structures of $[Al_4(HPO_4)_4(C_2H_5OH)_{12}]Cl_4{\cdot}4C_2H_5OH$ (compound **1**) and $[Al_4(HPO_4)_4(C_2H_5OH)_{12}]Br_4{\cdot}4C_2H_5OH$ (compound **2**) were obtained at low temperature. ^{13}C CP MAS NMR dynamics were carefully studied: non-exponential growth of magnetisation was observed for ^{13}C CP even for moderately coupled $^{13}CH_3$ groups. This approach was extended for the first time to ^{31}P CP MAS NMR. Variable contact time as well as inversion recovery cross polarisation (IRCP) experiments showed unambiguously that the $^1H \longrightarrow {}^{31}P$ magnetisation transfer was also not exponential. The ^{31}P IRCP MAS experiment proved to be a powerful tool for the study of complex amorphous materials, allowing editing of the spectra. Variable contact time experiments under fast MAS led to the observation of strong dipolar oscillations. The subsequent analysis of the CP data in the frequency domain led to the direct accurate determination of ^{31}P–^1H distances. This approach can be used as an alternative method for the measurement of distances in solid state NMR. ^{27}Al NMR quadrupolar parameters for **1** and **2** were derived by using several static and MAS techniques, in both time and frequency domains. The time domain response to a two-pulse sequence led to the very unusual observation of multiple quadrupolar Solomon echoes. The spectroscopic data related to **1** and **2** are a good starting point and pertinent tools for the study of more complex derivatives.

Introduction

Since the first successful synthesis of crystalline microporous aluminophosphate in 1982,[1] Group 13 (B, Al, Ga, In) metallophosphates have been extensively studied, owing to their potential catalytic and sorptive properties. This extended family of compounds includes $AlPO_4$-n structures,[2] large pore aluminophosphates like VPI-5 and JDF-20,[3,4] and gallophosphates like cloverite.[5] Research was undertaken to synthesise small building units with definite cores, corresponding to the secondary building units (SBUs) of the target materials. Several small boro-, alumino-, and gallo-phosphonate entities were successfully synthesised and characterised by X-ray diffraction or spectroscopic techniques. Among them, models for single four-ring (4R or 4) skeletons,[6] double four-ring (D4R or 4–4) skeletons,[6d–f,7] prismatic shaped clusters,[6a,e–f] and double six-ring (D6R or 6–6) skeletons[8] were obtained.

Most of the structures of inorganic cores described above were established by X-ray diffraction on single crystals and these compounds were often analysed by infrared spectroscopy and multinuclear solution state NMR spectroscopy. Surprisingly, although many aluminophosphate materials (including $AlPO_4$-n, lamellar[9] and mesoporous[10] Al–P derivatives) were investigated by ^{27}Al and ^{31}P solid state NMR techniques, the molecular SBU analogues described above were never investigated by *solid state* NMR. However, they can be considered as models for spectroscopic investigations, as small well defined molecules are involved. In that sense, such molecules can be compared to the cubane shaped silsesquioxanes,[11] which were intensely studied by vibrational spectroscopy and solid state NMR.[12]

In this paper, we present the complete study of tetrakis[μ_3-hydrogentetraoxophosphato(2−)]tetrakis[tris(ethanol)-aluminium](4+) chloride·ethanol(1/4): $[Al_4(HPO_4)_4(C_2H_5OH)_{12}]Cl_4{\cdot}4C_2H_5OH$ (compound **1**) and tetrakis[μ_3-hydrogentetraoxophosphato(2−)]tetrakis[tris(ethanol)aluminium](4+) bromide·ethanol(1/4): $[Al_4(HPO_4)_4(C_2H_5OH)_{12}]Br_4{\cdot}4C_2H_5OH$ (compound **2**). First, we present a short description of the crystallographic structures of **1** and **2**. The structure of **1** was partially resolved in 1975 by Cassidy *et al.*[13] and the structure of **2** has never been published in the literature. These compounds exhibit a double four-ring skeleton, similar to the D4R or 4–4 SBU occurring in zeolites. After a brief presentation of the ^{31}P solution NMR study, compounds **1** and **2** were systematically studied by *solid state* multinuclear NMR. ^{31}P and ^{13}C CP MAS dynamics were analysed in terms of *coherent* and *incoherent* transfer of magnetisation. Fast ^{31}P CP MAS experiment led to the observation of dipolar oscillations and to the *direct* estimation of P–H distances. Emphasis on the precise measurement of ^{31}P–^1H distances using CP is made: it was

Table 1 Crystallographic data for $[Al_4(HPO_4)_4(C_2H_5OH)_{12}]Cl_4 \cdot 4C_2H_5OH$ **1** and $[Al_4(HPO_4)_4(C_2H_5OH)_{12}]Br_4 \cdot 4C_2H_5OH$ **2**

Formula	$C_{32}H_{100}Al_4P_4O_{32}Cl_4$ **1**	$C_{32}H_{100}Al_4P_4O_{32}Br_4$ **2**
Formula weight	1370.8	1548.4
Crystal system	Tetragonal	Tetragonal
Space group	$I\bar{4}$	$I\bar{4}$
Colour	Colourless	Colourless
a/Å	15.379(8)	15.425(4)
b/Å	15.379(8)	15.425(6)
c/Å	14.410(3)	14.712(4)
α/°	90	90
β/°	90	90
γ/°	90	90
U/Å^3	3408(3)	3500(2)
T/K	233	163
Z	2	2
μ(Mo-Kα)/cm^{-1}	3.90	24.90
Measured reflections	1698	1743
Unique reflections	1574	1616
Used reflections	1179	1347
R_{int}	0.0600	0.0600
R^a	0.0623	0.0588
Rw	0.0749[b]	0.0725[c]

[a] $R = \Sigma||F_o| - |F_c||/\Sigma|F_o|$. [b] $w = w'[1 - (||F_o| - |F_c||/6\sigma(F_o))^2]^2$ with $w' = 1/\Sigma_r A_r T_r(X)$ with 3 coefficients 7.46, −0.195 and 5.71 for the Chebyshev series, for which X is $F_c/F_{c(max)}$. [c] $w = w'[1 - (||F_o| - |F_c||/6\sigma(F_o))^2]^2$ with $w' = 1/\Sigma_r A_r T_r(X)$ with 3 coefficients 11.1, −2.87 and 7.61 for the Chebyshev series, for which X is $F_c/F_{c(max)}$.

possible to evaluate with great accuracy phosphorus–hydrogen distances ranging from direct P–H bonds in phenylphosphinic acid to P–O–H bonds in compound **1**. This new approach should help in the exact location of protons in aluminophosphate/phosphonate frameworks. The use of high speed CP under MAS allows simultaneously high resolution and direct checking of the dipolar interaction between nuclei. In this way, our approach can be understood as an alternative to the more classical REDOR and TEDOR experiments.[14,15] Variants of the CP experiment (namely inversion recovery cross polarisation (IRCP)) were also used in this work. They showed unambiguously that the $^1H \longrightarrow {}^{31}P$ CP process must be analysed through the concept of *coherent/incoherent* transfer. This is the first time that such an analysis has been applied to ^{31}P CP spectroscopy. Then, ^{27}Al solid state NMR data are presented and discussed. The quadrupolar data were obtained with extreme accuracy by using several static and MAS techniques (three approaches): *i.e.* static 1D nutation, high speed MAS, and satellite transitions analysis. The obtained quadrupolar data did not fit obviously with C_Q values reported in the literature. Static two-pulse experiments led to the very unusual observation of multiple quadrupolar Solomon echoes in the time domain. These echoes can act as "fingerprints" for the various compounds.

We believe that such solid state NMR techniques can be easily generalised for the study of small inorganic clusters.

Results and discussion

Description of structures

We report the crystallographic structures of compounds **1** and **2** obtained at 233 K and 163 K, respectively. X-Ray diffraction data of compound **1** were reported by Cassidy *et al.*[13] in 1975 at room temperature. The exact location of the carbon atoms was not reported in the original work. To our knowledge, the crystallographic structure of compound **2** (Br derivative) was never published in the literature (although such a compound was evoked by Cassidy *et al.*).[13] Crystallographic data concerning compounds **1** and **2** are given in Table 1. Each structure consists of cubane shaped molecules, possessing $\bar{4}$ symmetry (see Fig. 1). Aluminium and phosphorus atoms are located alternatively at the vertices of the cube and they are linked by

Table 2 Selected bond distances (Å) and angles (°) for $[Al_4(HPO_4)_4(C_2H_5OH)_{12}]Cl_4 \cdot 4C_2H_5OH$ **1** and $[Al_4(HPO_4)_4(C_2H_5OH)_{12}]Br_4 \cdot 4C_2H_5OH$ **2**

1		**2**	
P1–O1	1.589(6)	P1–O1	1.581(8)
P1–O2	1.500(6)	P1–O2	1.507(7)
P1–O3	1.507(6)	P1–O3	1.497(7)
P1–O4	1.499(6)	P1–O4	1.507(8)
Al1–O2	1.799(5)	Al1–O2	1.822(7)
Al1–O3	1.812(7)	Al1–O3	1.804(8)
Al1–O4	1.833(6)	Al1–O4	1.820(8)
Al1–O5	1.969(6)	Al1–O5	1.953(7)
Al1–O6	1.973(6)	Al1–O6	1.974(8)
Al1–O7	1.959(6)	Al1–O7	1.935(7)
O5–Al1–O7	83.0(3)	O6–Al1–O7	83.8(3)
O2–Al1–O4	98.5(2)	O2–Al1–O3	98.3(3)
O1–P1–O3	106.0(4)	O1–P1–O2	102.8(4)
O2–P1–O4	114.0(3)	O2–P1–O3	112.9(4)

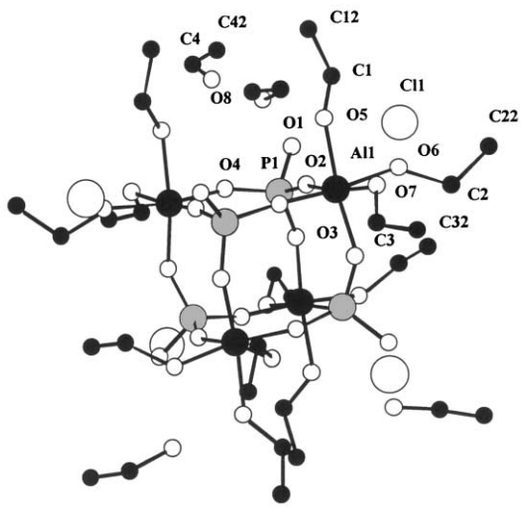

Fig. 1 A graphical view of the structure of $[Al_4(HPO_4)_4(C_2H_5OH)_{12}]Cl_4 \cdot 4C_2H_5OH$ **1**, showing the atom labelling scheme. H atoms are omitted for clarity. Compound **2** is isostructural with compound **1**.

bridging oxygen atoms along the edges of the cube (O2, O3, O4). Average bond lengths involving these bridging oxygen atoms are Al–O 1.81 Å and P–O 1.50 Å for both compounds **1** and **2** (see Table 2). The oxygen O1 atom is located outside the cage with P–O1 1.589(6) Å for compound **1** and 1.581(8) Å for compound **2**. These longer P–O1 bond lengths correspond to P–OH groups (see also the NMR section). Each halogen atom (Cl, Br) is located near three oxygen atoms, O1 and O6 (in the same cube) and O7 in a neighbouring cube, suggesting the existence of O–H ··· Cl(Br) hydrogen bonds (3.03–3.07 Å and 3.19–3.23 Å respectively). The aluminium atoms are octahedrally coordinated; three ethanol ligands are bonded to Al1 (*i.e.* C12C1O5, C22C2O6, and C32C3O7). The average Al–O bond length is 1.96 Å. The oxygen octahedra surrounding the aluminium atoms are distorted. In addition to the ethanol ligands bonded to the Al atoms, there are four more ethanol molecules associated with each cage unit (*i.e.* C42C4O8). We believe that the ethanol ligands, as well as the free ethanol molecules, prevent the linking of the cubane cores. Compounds **1** and **2** remain however very sensitive to air moisture (see Experimental section).

^{31}P solution NMR spectroscopy

Compounds **1** and **2** were dissolved in various solvents, *i.e.* EtOH, DMF and H_2O. In EtOH, the spectrum of compound **1** showed one major single resonance located at δ_P −23.6. The observed chemical shift is comparable to the one observed by ^{31}P CP MAS NMR spectroscopy (see below). The spectrum

of compound **2** in EtOH presents several resonances, in disagreement with the crystal structure (only one P site). It reflects the very high sensitivity of this compound towards water (especially when handling compound **2** in air). Compounds **1** and **2** seemed particularly "soluble" in H_2O (as mentioned by Cassidy *et al.*[13]) and DMF. However, the integrity of the cluster cages was not preserved in either solvent: several ^{31}P resonances of various intensities were observed.

^{13}C and ^{31}P solid state NMR spectroscopy

CP experiments and CP dynamics. CP dynamics ($^1H \longrightarrow X$) is classically studied by variable contact time experiments. When the ^1H–^1H interactions far exceed the heteronuclear dipolar coupling constants, the magnetisation transfer is then comparable to a relaxation process and is called *incoherent*. The X magnetisation evolution is then characterised by two time constants, following:[16]

$$M_X(t_{CP}) = \frac{\gamma_{^1H}}{\gamma_X} M_0 \frac{1}{1-\lambda}[1 - \exp(-(1-\lambda)t_{CP}/T_{XH})]\exp(-t_{CP}/T_{1\rho}(^1H)) \quad (1)$$

t_{CP} corresponds to the contact time, M_0 corresponds to the X Zeeman magnetisation, $\lambda = T_{XH}/T_{1\rho}(^1H)$ where T_{XH} stands for the cross relaxation time constant; $T_{1\rho}(^1H)$ is the relaxation time of protons in the rotating frame. When the X–^1H dipolar constant is comparable to the ^1H–^1H interactions, eqn. (1) is no longer valid. This is the case for rigid XH_n groups. CP is no longer a single-exponential process but proceeds in two stages with quite different time scales[17] and a quantitative expression for the polarised X magnetisation is given by (neglecting $T_{1\rho}(^1H)$):

$$M_X(t_{CP}) = \frac{\gamma_{^1H}}{\gamma_X} M_0 \left[1 - \frac{1}{n+1}\exp\left(-\frac{t_{CP}}{T_D}\right) - \frac{n}{n+1}\exp\left(-\frac{3}{2}\frac{t_{CP}}{T_D}\right)\exp\left(-\frac{t_{CP}^2}{T_C^2}\right)\right] \quad (2)$$

n corresponds to the number of directly bonded protons. T_C accounts for the *coherent* transfer of magnetisation involving the X nucleus and the directly bonded protons. T_D is related to the spin-diffusion process, which involves all remaining protons. Usually $T_D \gg T_C$. It follows from eqn. (2), that a quasi-equilibrium state, corresponding to $(n/n + 1)(\gamma_{^1H}/\gamma_X)M_0$, is rapidly obtained. Such a behaviour was demonstrated experimentally for rigid ^{13}CH and $^{13}CH_2$ groups.[17b,18]

^{13}C CP MAS NMR. The typical behaviour of the $^{13}CH_2$ magnetisation evolution *versus* t_{CP} (compound **1**) is presented in Fig. 2a. Two regimes are clearly observed and a quasi-equilibrium value (2/3; $n = 2$) is attained after several tens of microseconds. The fit derived from eqn. (2) (using $n = 2$) is in excellent agreement with the experimental data and leads to characteristic values for T_C and T_D. Considering $^{13}CH_3$ groups, the magnetisation evolution for δ_C 18.31 is presented in Fig. 2b (compound **1**). Two regimes of polarisation are clearly observed. No single exponential fitting procedure can describe fully the experimental data. Although it was generally admitted in the literature that the magnetisation evolution for $^{13}CH_3$ groups ($n = 3$) proceeded through an exponential process[19] (reduction of the dipolar coupling strength due to fast reorientation), more recently it was observed that $^{13}CH_3$ magnetisation evolved with two regimes of polarization.[20,21] Therefore, it is concluded that even for moderately coupled sites ($^{13}CH_3$), non-exponential behaviour during variable contact time experiments are observed. In other words, the transfer of magnetisation occurs first between the ^{13}C nuclei and the neighbouring protons and then with the more remote protons.

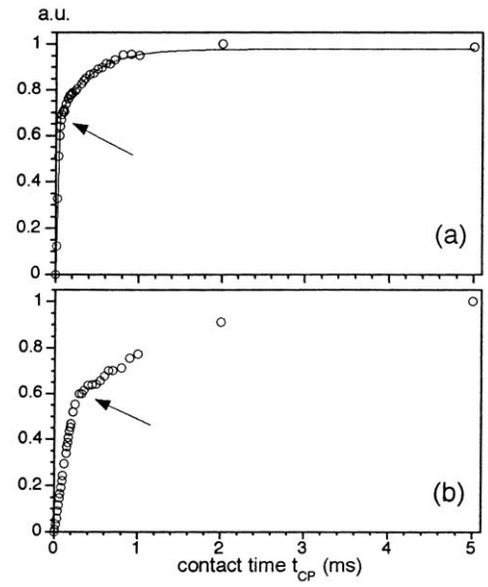

Fig. 2 Variable contact time experiment (^{13}C) for compound **1**. ν_{rot} = 4000 Hz; $\Xi(^{13}C)$ = 75.43 MHz; N_s (number of scans) = 800 (for each t_{CP} value); r.d. (recycle delay) = 5 s. ^1H high-power decoupling. Arrows indicate the quasi-equilibrium states. (a) Characteristic evolution for $^{13}CH_2$ magnetisation (δ 59.06). Fit using eqn. (2) ($n = 2$) with T_C = 27 ± 1 μs and T_D = 0.38 ± 0.03 ms. (b) Characteristic evolution for $^{13}CH_3$ magnetisation (δ 18.31).

^{31}P CP MAS NMR. ^{31}P CP dynamics is studied using the same approach, keeping in mind the *coherent/incoherent* processes of transfer. For compounds **1** and **2**, ^{31}P CP MAS experiments were used especially for relaxation considerations ($T_1(^{31}P) \geq 98$ s at 7.04 T) and for the fine description of the ^{31}P–^1H heteronuclear dipolar interaction. Resonances located at δ_P −25.7 and −26.6 are observed for compounds **1** and **2** respectively (Table 3). CSA (chemical shift anisotropy) parameters are $\Delta\delta \approx 62$ and 66 ppm for compounds **1** and **2**, respectively (Table 3). These rather large anisotropies are due primarily to the protonation of the phosphate groups. However, these CSAs are much smaller than those observed for hydrogenophosphates such as $CaHPO_4{\cdot}2H_2O$.[22] Moreover, it is interesting to note that these values cannot be related to the distortion d of the $[PO_3(OH)]^{2-}$ tetrahedra defined by:[23]

$$d = \frac{\sum^{n}(109.5° - \theta)}{n} \quad (3)$$

where θ stands for the various O–P–O angles. For compounds **1** and **2**, $d \approx 3.5$. This would imply a CSA higher than 100 ppm, which is obviously not observed.[23]

Variable contact time experiments for compounds **1** and **2** are presented in Fig. 3. Very few data concerning the ^{31}P CP dynamics are available in the literature.[24,25] These data were generally analysed in terms of *incoherent* magnetisation transfer (see eqn. (1)). Fig. 3 shows obviously that several regimes of polarisation during the CP transfer are present. The ^{31}P magnetisation evolves rapidly during the first hundreds of μs (*i.e.* $0 \leq t_{CP} \leq 200$ μs). Then, the ^{31}P magnetisation evolves more slowly for 200 μs $\leq t_{CP} \leq$ 10 ms ($T_{1\rho}(^1H)$ effects can be neglected). Moreover, it is very surprising to note that *ca.* half of the total magnetisation is attained after the rapid regime of polarisation, for both compounds **1** and **2**. Such multi-component behaviour has been reported in the literature.[24,25] The authors suggested that several T_{CH} and $T_{1\rho}(^1H)$ values should be considered in connection with eqn. (1) for an accurate description of the CP transfer. We believe that the multi-step growth of the magnetisation is characteristic of ^{31}P–O–^1H groups and that the rapid increase during the first hundreds of μs is related to

Table 3 ^{27}Al, ^{13}C and ^{31}P NMR data for $[Al_4(HPO_4)_4(C_2H_5OH)_{12}]Cl_4\cdot 4C_2H_5OH$ **1** and $[Al_4(HPO_4)_4(C_2H_5OH)_{12}]Br_4\cdot 4C_2H_5OH$ **2**, including isotropic chemical shift (δ_{iso}, ppm), linewidth (LW, Hz), quadrupolar coupling constant (C_Q, MHz), asymmetry parameter (η_Q), shielding tensor components (δ_{ii}, ppm), asymmetry parameter (η_{CSA})[a]

		1	**2**
^{27}Al	δ_{iso}	−8.7[b]; −8.8[c]	−8.2[b]; −8.2[d]
	C_Q	1.69[e]; 1.77[b]; 1.67[c]	1.81[e]; 1.86[b]; 1.84[d]
	η_Q	0.30	0.25
^{13}C	δ_{iso} CH_3 (LW)	17.13 (11); 17.36 (9); 17.79 (10); 18.31 (10)	16.55 (25); 17.11 (23); 17.76 (26); 18.04 (26)
	δ_{iso} CH_2 (LW)	58.74 (19); 59.06 (31); 59.76 (36); 61.17 (38)	58.64 (64); 59.46 (54); 60.26 (47); 61.39 (79)
^{31}P	δ_{iso} (LW)	−25.7 (250)	−26.6 (256)
	δ_{11}; δ_{22}; δ_{33}[f]	−60.9; −31.8; 15.7	−61.8; −35.5; 17.4
	η_{CSA}[f]	0.70	0.60

[a] δ in ppm; $\delta_{iso} = (1/3)(\delta_{11} + \delta_{22} + \delta_{33})$ with $|\delta_{33} - \delta_{iso}| \geq |\delta_{11} - \delta_{iso}| \geq |\delta_{22} - \delta_{iso}|$; $\eta_{CSA} = (\delta_{22} - \delta_{11})/(\delta_{33} - \delta_{iso})$; $\Delta\delta = \delta_{33} - (\delta_{11} + \delta_{22})/2$; $C_Q = (e^2qQ)/h$; $\delta_{iso}(^{27}Al)$[b,d]: ± 0.1; $\delta_{iso}(^{13}C)$: ± 0.02 (**1**), ± 0.05 (**2**); $\delta_{iso}(^{31}P)$: ± 0.1; η_{CSA}, η_Q: ± 0.05; C_Q[b,d]: ± 0.01 MHz. [b] From the fitting of the central transition powder pattern under fast MAS (7.04 T). [c] From SORGE diagram[42] (Fig. 9). [d] From the fitting of the central transition powder pattern under fast MAS (9.4 T.) (±3/2 ↔ ±5/2) satellite transitions are not clearly observed. [e] From static nutation experiments (Fig. 6). [f] δ_{ii} and η_{CSA} from MAS sidebands pattern analysis.

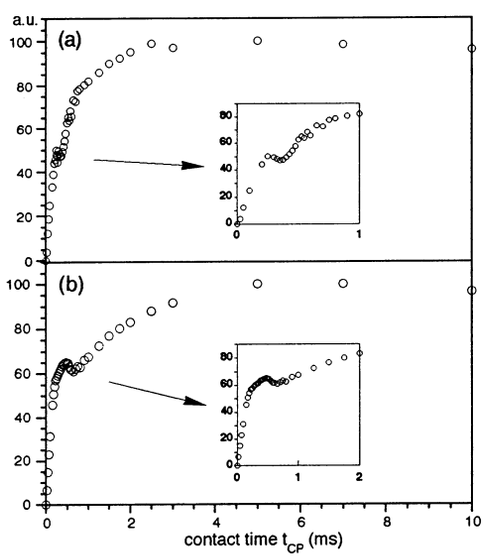

Fig. 3 Variable contact time experiment (^{31}P) for compounds **1** (a) and **2** (b). ν_{rot} = 5000 Hz; $\Xi(^{31}P)$ = 121.44 MHz; N_s = 40 (for each t_{CP} value); r.d. = 5 s. ^{1}H high-power decoupling.

coherent transfer between ^{31}P and ^{1}H. Therefore, the model described by eqn. (2) seems to be more accurate for the description of the ^{31}P magnetisation. To our knowledge, this is the first time that *coherent*/*incoherent* transfer of magnetisation has been involved in ^{31}P CP NMR studies. More surprisingly, oscillations located at $t_{CP} \approx 300$ μs and $t_{CP} \approx 400$ μs are observed for compounds **1** and **2**, respectively. These oscillations are severely damped but are still visible. Such oscillations have been reported in ^{13}C CP MAS NMR (involving the ^{13}C–^{1}H heteronuclear dipolar interaction) and oscillations due to ^{13}C–^{31}P cross polarisation between isolated spin pairs have been reported once in the literature.[26] In our work, the study of these oscillations (^{31}P–^{1}H) was undertaken under fast MAS.

^{31}P CP dynamics under fast MAS: direct determination of ^{31}P–O–^{1}H and ^{31}P–^{1}H distances. As shown above, highly damped oscillations in the ^{31}P CP variable contact time experiment are observed (Fig. 3) under moderate MAS (*i.e.* 5 kHz). In order to enhance the oscillations and slow down the ^{1}H–^{1}H spin diffusion process, CP experiments at fast MAS (*i.e.* 14.1 kHz) were performed. Following Bertani *et al.*,[27] it is known that under fast MAS conditions, the H–H profile splits into sidebands at $\Delta = \omega_1(^1H) - \omega_1(^{31}P) = \pm n\omega_r$,[30] where ω_r corresponds to the rotor angular velocity. Efficient CP occurs at $n = \pm 1$ and $n = \pm 2$. We define the heteronuclear dipolar constant by:

$$D_{^1H^{31}P} = \mu_0\, \gamma_{^{31}P}\, \gamma_{^1H}\, \hbar/(4\,\pi r_{PH}^3) \quad (4)$$

At the $n = \pm 1$ and $n = \pm 2$ sideband matching conditions and assuming $\omega_r \gg D_{^1H^{31}P}$, it can be proved that the transferred magnetisation is given by (neglecting spin–lattice relaxation in the rotating frame $T_{1\rho}$ and ^{1}H–^{1}H/^{31}P–^{31}P spin diffusion):[31]

$$M_{^{31}P}(t) = \frac{\gamma_{^1H}}{2\gamma_{^{31}P}} M_0[1 - \cos(\delta_n t)] \quad (5)$$

with

$$\delta_{\pm 1} = (D_{^1H^{31}P}\sqrt{2}\,\sin 2\beta)/4 \quad (6a)$$

$$\delta_{\pm 2} = (D_{^1H^{31}P}\sin^2\beta)/4 \quad (6b)$$

β is the angle between the P–H internuclear vector and the rotor axis. For a powder sample, and $n \pm 1$, the weighting of β has to be taken into account and the following integral must be evaluated for various t_{CP} values :

$$O(t_{CP}) = \int_0^{\pi/2}\left[1 - \cos\left(\frac{D_{^1H^{31}P}\, t_{CP}\sqrt{2}\,\sin 2\beta}{4}\right)\right]\sin\beta\; d\beta \quad (7)$$

This particular integral may be evaluated by using the NIntegrate routine of *Mathematica*.[52] $O(D_{^1H^{31}P}\ t_{CP})$ is represented in Fig. 4a. As shown by Bertani *et al.*,[27] the Fourier transform of $O(D_{^1H^{31}P}t_{CP})$ leads to a Pake-like powder pattern, without lateral wings (Fig. 4b). The dipolar constant $D_{^1H^{31}P}$ is then *directly* derived, as the maximum splitting in the Pake-like powder pattern corresponds to $D_{^1H^{31}P}/\sqrt{2}$.

To this point, it is important to notice that eqn. (5) to (6b) were derived assuming $\omega_r \gg D_{^1H^{31}P}$, where ω_r is related to the MAS rotation frequency of the sample. Recently, Bertani[28] studied in detail this CP MAS experiment and the subsequent Fourier transform, assuming $\omega_r \approx D_{^1H^{31}P}$. For $D_{^1H^{31}P}$ = 15 kHz (this value is comparable to that observed in the case of the phenylphosphinic acid, $H(C_5H_6)PO(OH)$–see below) and $\omega_r \geq$ 8 kHz, it was proved numerically that the obtained Pake-like powder pattern still has well-defined horns (see Fig. 4b) allowing the correct estimation of the dipolar constant. In this case, sharp spinning side bands are located around the central doublet. It follows that the experimental approach described above is still valid for $\omega_r \approx D_{^1H^{31}P}$. For $\omega_r \leq 4$ kHz, the analysis of the central doublet is strongly obscured by the presence of complex side band patterns.

Finally, it must be noted that rotary resonance effects have

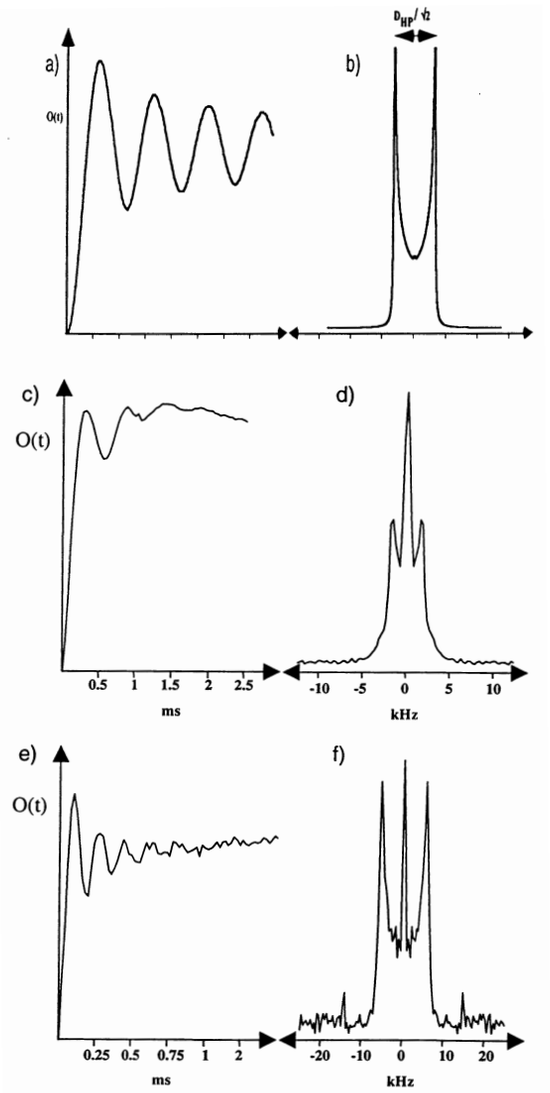

Fig. 4 $^{1}H/^{31}P$ cross polarisation dynamics under fast MAS. (a) Theoretical time evolution at the $n = \pm 1$ Hartmann–Hahn condition for an isolated two-spin 1/2 system. (b) Fourier transform of (a) after multiplication by −1, baseline correction and slight apodization. (c) Experimental time evolution at $\omega_r/2\pi = 14.1$ kHz for compound **1** with $\omega_1(^{1}H)/2\pi = 46.7$ kHz and $\omega_1(^{31}P)/2\pi = 32.7$ kHz. $\Xi(^{31}P) = 80.96$ MHz; $N_s = 48$ (for each t_{CP} value, 44 increments); r.d. = 7 s. ^{1}H high-power decoupling. (d) Fourier transform of (c) after multiplication by −1, baseline correction and zerofilling with no line broadening. (e) Experimental time evolution at $\omega_r/2\pi = 14.1$ kHz for the phenylphosphonic acid $H(C_6H_5)PO(OH)$. (f) Fourier transform of (e) after multiplication by −1, baseline correction and zerofilling with no line broadening.

already been demonstrated in solid state NMR.[32] Pseudo Pake doublets were also observed, but in the frame of double-quantum 2D experiments. The method presented in this article is much easier to implement and it was shown[27] that the positions of the horns of the Pake-like powder pattern were rather insensitive to experimental missettings. The variable contact time curve for compound **1** at 14.1 kHz is presented in Fig. 4c. Oscillations are much more pronounced than those observed at 5 kHz. The Fourier transform is also presented in Fig. 4d. The derived splitting is 3.5 kHz. This corresponds to a $^{31}P–O–^{1}H$ distance of 2.1 ± 0.1 Å. By considering the crystallographic data given above and assuming d(O–H) ≈ 1 Å, the P–O–H angle is evaluated to be 107 ± 8°. Such a value is in agreement with X-ray and neutron diffraction data.[33] The central peak, superimposed on the Pake pattern (Fig. 4d), is explained by the remaining spin diffusion process. Indeed, the role of spin diffusion can be explained as follows:[18,29] (i) the spin diffusion tends to damp the dipolar oscillations, leading to a broadening of the Pake-like powder pattern in the frequency domain. (ii) The exponential character of the incoherent transfer of magnetization by spin diffusion (leading to the final equilibrium state) is related to a central peak (at 0 kHz) after Fourier transformation. At 14.1 kHz, we conclude therefore that the spin diffusion process is not totally suppressed for compound **1**. However, the assumption of a spin pair is in this case sufficient for explaining the experimental data. The analysis of the data by using eqn. (5) to (6b) seems correct.

The fast CP MAS approach was also applied successfully to the study of the phenylphosphinic acid, $H(C_5H_6)PO(OH)$ (see Experimental section). This compound exhibits a direct short P–H bond. The corresponding 14.1 kHz CP MAS experiment is presented in Fig. 4e. Very well-marked oscillations are observed, leading to the following distance estimation (Fig. 4f): $d(^{31}P–^{1}H) = 1.46 \pm 0.02$ Å. This value is in very good agreement with previously published data.[34]

We believe that the described recoupling technique under fast MAS is very promising for the characterisation of P–OH or P–H in aluminophosphates or related materials. The direct location of protons in the structures becomes possible. As the experiment is performed under fast MAS, ^{31}P high resolution is obtained, enabling the individual characterisation of each ^{31}P site.

^{31}P inversion recovery cross polarisation (IRCP) experiments. Application to amorphous compounds. Various solid state NMR sequences were proposed in the literature, which allow the precise study of the CP dynamics or the partial editing of spectra, based on the heteronuclear dipolar interaction. First introduced by Melchior,[35] the IRCP sequence (Fig. 5a) has been widely used in the frame of ^{13}C CP MAS experiments.[17–20] It has been demonstrated that CP and IRCP dynamics are identical. However, this inversion technique presents the following advantages over variable contact time experiments: the inversion of polarisation occurs after a long contact time, thereby enhancing the signal to noise ratio. It follows that subtle CP behaviour can be observed even in the case of strongly overlapping lines. The rate of inversion is directly related to the involved dipolar coupling. In the case of strongly coupled $^{13}C–H$ spin pairs, two regimes of inversion of magnetisation were observed: a rapid *coherent* transfer of magnetisation between ^{13}C and ^{1}H, followed by a much slower *incoherent* transfer. To our knowledge, this work deals for the first time with ^{31}P IRCP MAS NMR spectroscopy. The IRCP evolution *versus* t_i of compounds **1** and **2** are presented in Fig. 5b and c. Two regimes of inversion are clearly observed, in agreement with the CP behaviour described above. It proves unambiguously that $^{31}P–O–^{1}H$ groups may be characterised by CP and IRCP experiments and that two-stage evolutions are observed in both cases. The IRCP sequence was then applied to the study of an amorphous compound obtained after degradation of compound **1** in air. The ^{31}P CP MAS NMR spectrum of this compound is presented in Fig. 5d (top spectrum). A broad and featureless peak located at $\delta_P \approx -17$ is observed. For $t_i = 525$ μs (Fig. 5e), a second component (already inverted) is clearly observed and located at $\delta_P \approx -25$. This peak (corresponding to few % of the total line) may be safely assigned to $[PO_3(OH)]^{2-}$ groups whereas the main component ($\delta_P \approx -17$) can be assigned to totally condensed $[PO_4]^{3-}$ entities (the magnetisation related to these non-protonated groups inverts slowly). This editing of spectra would have been much more difficult (or even impossible) using standard variable contact time experiments. We believe that such an approach could help in the study of amorphous phosphate materials. Finally, it can be noted that the IRCP scheme may be used for the fine setting of the H–H condition, as proposed by Melchior[36] (see Experimental section).

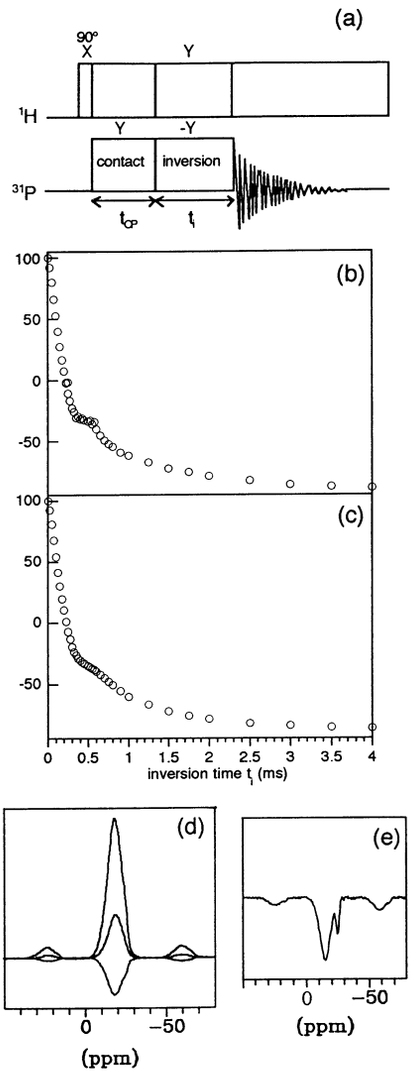

Fig. 5 Inversion recovery cross polarisation (IRCP) spectroscopy applied to ^{31}P MAS. ν_{rot} = 5000 Hz; $\Xi(^{31}P)$ = 121.44 MHz. (a) The IRCP pulse scheme. (b) Evolution of the magnetisation *versus* t_i for compound **1** (t_{CP} = 3 ms; N_s = 16). (c) Evolution of the magnetisation *versus* t_i for compound **2** (t_{CP} = 3 ms; N_s = 16). (d) IRCP sequence applied to the amorphous derivative of **1** (t_{CP} = 1 ms; N_s = 80). From top to bottom: standard CP experiment (t_i = 0 μs), t_i = 225 μs, and t_i = 1 ms. (e) As for (d), with N_s = 680 and t_i = 525 μs.

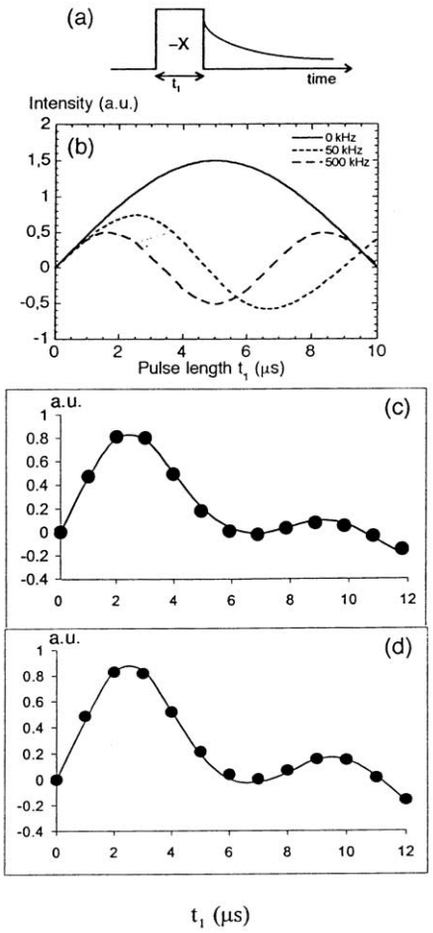

Fig. 6 Static ^{27}Al nutation experiment. $\omega_{RF}/2\pi$ = 50 kHz, corresponding to a π/2 pulse duration of 5 μs (from $Al(NO_3)_3$ solution); $\Xi(^{27}Al)$ (Larmor frequency) = 78.17 MHz; N_s = 12000 (for each t_1 pulse length); r.d. = 1 s. No ^{1}H high-power decoupling. Phase correction is applied for the spectrum corresponding to t_1 = 2 μs; the obtained parameters are then applied to the other spectra. (a) The one-pulse scheme used. (b) Relative intensity of the central line *versus* the RF pulse length t_1 for several values of $\omega_Q/2\pi$: 0, 50, and 500 kHz. $\omega_Q = (3\pi/40)\, C_Q\, (3\cos^2\beta - 1 + \eta_Q \sin^2\beta \cos 2\alpha)$ with $C_Q = e^2qQ/h$. α and β are the Euler angles describing the orientation of the strong magnetic field B_0 in the principal axis system (PAS) of the electric field gradient (EFG) tensor. For very small ($\omega_{RF}t_1$) values, the intensity becomes independent of ω_Q/ω_{RF}. In this regime, quantitative measurements of relative quadrupolar nuclei populations are obtained. (c) 1D nutation and the corresponding simulation using C_Q = 1.69 MHz and $\omega_{RF}/2\pi$ = 56.8 kHz for compound **1**. (d) 1D nutation and the corresponding simulation using C_Q = 1.81 MHz and $\omega_{RF}/2\pi$ = 54.7 kHz for compound **2**. η_Q is fixed in both cases to 0.3.

^{27}Al solid state NMR spectroscopy

One pulse static experiment: ^{27}Al nutation of compounds 1 and 2. Solid state NMR experiments dealing with quadrupolar nuclei can be divided into two groups: the first one deals with lineshape studies in the frequency domain (see below). The second one deals with the response of the spin system to radiofrequency (RF) pulses in the time domain. The simplest sequence (Fig. 6a) applied to a quadrupolar nucleus corresponds to a single pulse with variable duration t_1 (*i.e.* 1D nutation).[37] Analytical expressions for spin 5/2 (^{27}Al) line intensities were derived.[38] Precise determination of the quadrupolar coupling constant (C_Q or ω_Q) and asymmetry parameter (η_Q) are obtained for single-site compounds such as **1** and **2**. The evolution of line intensity *versus* t_1 is presented in Fig. 6b. The key parameter is ω_Q/ω_{RF} (at fixed ω_{RF}, it defines the so-called "nutation regime"). In other words, for $\omega_Q \ll \omega_{RF}$ or $\omega_Q \gg \omega_{RF}$, sinusoidal behaviour of the magnetisation is observed. For $\omega_{RF} \approx \omega_Q$, the evolution is clearly aperiodic. When dealing with powders, a distribution of ω_Q is expected. Assuming $C_Q \approx 2$ MHz and η_Q = 0.3 (see below), it follows that $|\omega_Q/2\pi|$ is in the range [0; 170 kHz]. It is possible to simulate the nutation curve of a powdered sample, after integration of the total intensity of the central transition *versus* t_1. The nutation curves of powdered compounds **1** and **2** are presented in Fig. 6c and 6d, respectively. Only the broad and featureless central transition is observed (the powder patterns of the outer ($m - 1 \leftrightarrow m$) transitions with $m \neq 1/2$ are very broad and cannot be detected). The *shift* of the central transition is independent of the first-order quadrupolar interaction but its *intensity versus* t_1 is not. Both curves are aperiodic, indicating that C_Q values are intermediate between high and very low values. Indeed, fitted values for C_Q are 1.69 MHz and 1.81 MHz for compounds **1** and **2**, respectively (Table 3). Finally, one can note that the best fits are obtained for reduced volumes of sample within the rotor: RF magnetic field inhomogeneities affect strongly the integration of the lines.

Two-pulse static experiment: ^{27}Al Solomon echoes. In the study of quadrupolar nuclei, broad powder patterns (corre-

sponding for instance to the satellite transitions) are often distorted by the dead time of the receiver of the spectrometer. In order to recover the lost signal, a two-pulse spin-echo sequence is commonly applied. In this work, two in phase pulses {–X}–τ_2–{–X}–[detection] (Fig. 7a) were used for the study of compounds **1** and **2**. The interpulse delay τ_2 verified $\tau_2 \ll T_{FID}$ (T_{FID} corresponds to the decay of the FID after a single pulse). Usually, a single echo is obtained after a two-pulse sequence. This echo (or half of the echo) can be subsequently Fourier transformed, leading to an undistorted lineshape in the frequency domain. The time domain response of the spin system (compound **1**) to the echo sequence is presented in Fig. 7c. Obviously, three echoes are observed (similar results are obtained for compound **2**) corresponding to the so-called Solomon echoes.[39] The origin, positions in the time domain, and amplitudes of the echoes were precisely defined and calculated.[40] The signals **A**, **B**, and **C** correspond to echoes of the satellite transitions and are superimposed on the FID signal (central transition). For each satellite transition ($\pm(m - 1) \leftrightarrow \pm m$), $(4I^2 - 1)/8$ echoes should be present. Among them, *allowed* echoes correspond to the refocusing of two 1Q (single quantum) and 2 MQ (multiple quantum) coherences and *forbidden* echoes correspond to the refocusing of four MQ coherences. For ^{27}Al ($I = 5/2$) and the ($\pm 1/2 \leftrightarrow \pm 3/2$) satellites, three echoes should be observed, located at $\tau_4 = \tau_2$, $2\tau_2$, and $3\tau_2$,[40] the last one being a forbidden one. For the ($\pm 3/2 \leftrightarrow \pm 5/2$) satellites, three echoes should be observed as well, located at $\tau_4 = \tau_2/2$, τ_2, and $3\tau_2/2$, the last one being a forbidden one. The

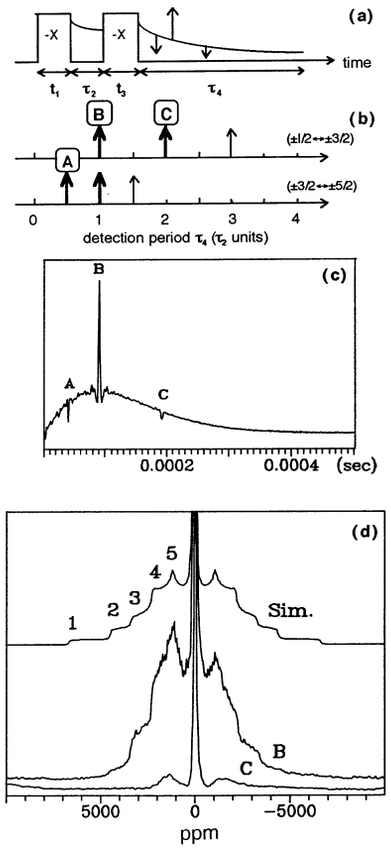

Fig. 7 Two-pulse ^{27}Al static experiment. $\Xi(^{27}Al)$ = 78.17 MHz. The echoes are clearly observed after a few hundreds of scans. No ^{1}H high-power decoupling. (a) The two-pulse scheme used. (b) Location of the echoes in the detection period τ_4.[38] Thick arrows correspond to allowed echoes (**A**, **B**, **C**); thin arrows correspond to forbidden echoes. (c) Experimental observation of echoes **A**, **B**, **C** for compound **1** ($t_1 = t_3 = 1.5$ μs and $\tau_2 = 100$ μs, $\omega_{RF}/2\pi = 50$ kHz, $N_S = 154000$, r.d. = 1 s). (d) Fourier transform of the **B** echo after line broadening (LB = 5000). Fourier transform of the **C** echo. Simulated powder pattern using $C_Q = 1.73$ MHz and $\eta_Q = 0.3$.

positions of the different echoes in the τ_4 time domain are presented in Fig. 7b. To our knowledge, multiple echoes for ^{27}Al have only been reported once in the literature, and were hardly discernible.[41] In Fig. 7c, the three echoes located at $\tau_4 = \tau_2/2$, τ_2, and $2\tau_2$ are clearly observed and correspond to allowed echoes. We can note that echo **A** is much sharper than echoes **B** and **C**: it corresponds to the more broadened satellites in the frequency domain, *i.e.* ($\pm 3/2 \leftrightarrow \pm 5/2$). At this stage, the presence of multiple echoes indicates that the chemical environment of ^{27}Al in compounds **1** and **2** is sufficiently distorted to create non-zero EFG. Solomon echoes can be thought of as a "fingerprint" of the quadrupolar interaction at the Al site. Moreover, C_Q must be rather small, as Solomon echoes are directly related to satellite transitions. When C_Q is large, satellites are smeared over the MHz range and no Solomon echo is detected. In order to derive more information from the multiple echoes, a Fourier transformation was applied to the various echoes. The Fourier transformation of the right-hand half of echo **B** led to a very distorted spectrum with strong oscillations. This is due to the presence of the **C** echo. When line-broadening is applied, the echo **C** is strongly reduced and Fourier transformation then seems valid. The obtained spectrum is presented in Fig. 7d. It corresponds to the powder pattern of *both* pairs of satellite transitions. This spectrum can be accurately simulated by the sum of the ($\pm 1/2 \leftrightarrow \pm 3/2$) and ($\pm 3/2 \leftrightarrow \pm 5/2$) satellite contributions. The discontinuities ($2 \longrightarrow 5$) are clearly observed. As the discontinuities of a quadrupolar powder pattern are very sensitive to the asymmetry parameter, η_Q is precisely derived (0.3). Moreover, the extension of the powder pattern in the frequency domain directly provides $C_Q = 1.73$ MHz. Only the (1) discontinuity is not detected (($\pm 3/2 \leftrightarrow \pm 5/2$) satellites). The Fourier transformation of the right-hand half of echo **C** led to the powder pattern shown in Fig. 7d. It corresponds to the ($\pm 1/2 \leftrightarrow \pm 3/2$) satellite powder pattern. The (5) discontinuity is observed. It has been shown that the Fourier transformation of the different echoes lead either to the sum or to the individual satellite powder patterns.

Slow and fast MAS experiments. The complete spinning sidebands patterns for satellite transitions may be observed and fully analysed in terms of quadrupolar coupling constant C_Q and asymmetry parameter η_Q.[42] Such a detailed analysis allows the determination of the "true" chemical shift δ_{iso} of a given Al site, corrected for second-order induced shifts. The central transition under fast MAS conditions (ν_{rot} = 14 kHz) is presented in Fig. 8b (compound **1**). A typical second-order broadened lineshape is observed. Discontinuities, including the edge on the right-hand side of the powder pattern, are clearly seen and allow the precise determination of C_Q, η_Q, and δ_{iso}. These values are reported in Table 3. To our knowledge, very few well resolved lines with rather small quadrupolar constants ($C_Q < 2$ MHz) have been published in the literature.[41] At ν_{rot} =

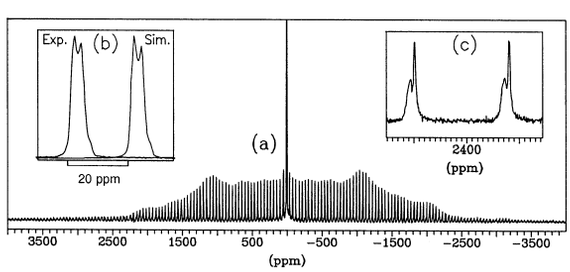

Fig. 8 ^{27}Al MAS experiments for compound **1**. $\omega_{RF}/2\pi = 50$ kHz; pulse flip angle: ≤ π/12; ν_{rot} = 3570 Hz and 14000 Hz; $\Xi(^{27}Al)$ = 78.17 MHz; N_s = 1300; r.d. = 1s. ^{1}H high-power decoupling. (a) The manifold of spinning sidebands from the satellite transitions. (b) The center band of the central transition and its simulation using $C_Q = 1.77$ MHz and $\eta_Q = 0.3$. (c) The partial resolution of the ($\pm 1/2 \leftrightarrow \pm 3/2$) (thin lines) and ($\pm 3/2 \leftrightarrow \pm 5/2$) (broad lines) satellite transitions.

14 kHz, we assume that the heteronuclear (^{27}Al–^{31}P) and homonuclear (^{27}Al–^{27}Al) dipolar interactions are totally removed. Quite surprisingly, high-power ^{1}H decoupling is necessary for the clear observation of the various discontinuities. This is in agreement with the presence of H nuclei in the vicinity of Al atoms (see Crystallographic section). The low speed MAS spectrum of compound **1** is presented in Fig. 8a (ν_{rot} = 3.57 kHz). Interestingly, each sideband corresponds to the sum of two peaks, which are almost separated: they correspond to the much less intense inner (±1/2 ↔ ±3/2) and outer (±3/2 ↔ ±5/2) satellite transitions. Partial resolution of the spinning sidebands for satellite transitions (Fig. 8c) is due to second-order quadrupolar shifts.[42] Very few examples of this particular splitting have been reported in the literature, in the frame of ^{27}Al MAS spectroscopy.[43] It has been shown that the knowledge of the centre of gravity of the central transition and satellite transitions $\delta_{CG}^{\langle m \rangle}$ allows the direct determination of δ_{iso} and $\nu_{Q(\eta_Q)}$, where:

$$\nu_{Q(\eta_Q)} = \nu_Q \sqrt{1 + \frac{\eta_Q^2}{3}} \quad (8a)$$

$$\nu_Q = \frac{3}{2I(2I-1)} C_Q \quad (8b)$$

The equation relating $\delta_{CG}^{\langle m \rangle}$, δ_{iso}, and $\nu_{Q(\eta_Q)}$ is given by:

$$\delta_{CG}^{\langle m \rangle} = \delta_{iso} - [\nu_{Q(\eta_Q)}]^2 \frac{[I(I+1) - 3 - 9\,m(m-1)]\,10^6}{30\,\nu_0^{\,2}} \quad (9)$$

Eqn. 9 can be represented graphically, leading to the so-called second order graphic extrapolation or SORGE diagram.[44] The values of $\delta_{CG}^{\langle m \rangle}$ for m = 1/2, 3/2, and 5/2 are plotted versus ($[I(I + 1) - 3 - 9m(m - 1)]\ 10^6/(30\nu_0^2)$ in Fig. 9. The slope of

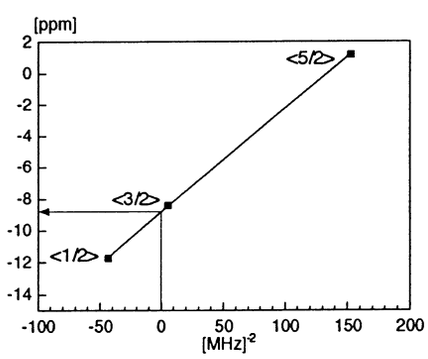

Fig. 9 SORGE diagram[42] for compound **1**. $\delta_{CG}^{\langle m \rangle}$ (m = 1/2, 3/2, and 5/2) are plotted versus $X = [I(I + 1) - 3 - 9m(m - 1)]10^6/(30\nu_0^2)$ (see text). For $X = 0$, the value of δ_{iso} is directly evaluated.

the obtained line gives $[\nu_{Q(\eta_Q)}]^2$, and for an "infinite" field, one derives δ_{iso}. The experimental values are: $\nu_{Q(\eta_Q)}$ = 0.256 MHz or ν_Q = 250 kHz (*i.e.* C_Q = 1.67 MHz), assuming η_Q = 0.3 (see above), and $\delta_{Al\ iso} = -8.7$ ppm. All characteristic parameters for compounds **1** and **2** are given in Table 3.

As a conclusion, C_Q and η_Q parameters for cubanes **1** and **2** were precisely determined using many independent experiments in both time and frequency domains. It can be noted further that the separation of the inner and outer satellites (compound **1**) is an accurate test for the setting of the magic angle during the experiment. The obtained parameters for compounds **1** and **2** are good starting points for the understanding of chemical reactions between the molecular moieties or of the evolution of these compounds in air. Moreover, the C_Q parameters for compounds **1** and **2** can be compared to values already published for various ^{27}Al sites. According to Ghose *et al.*,[45] the quadrupolar coupling constant of octahedrally coordinated Al increases with the longitudinal strain $|a|$ defined by:

$$|a| = \Sigma|\ln(l_i/l_0)| \quad (10)$$

where l_i is the individual Al–O bond length and l_0 is the ideal bond length of a perfect polyhedron with the same volume as the distorted polyhedron. The $|a|$ values for the various ^{27}Al sites for compounds **1** and **2** are reported in Fig. 10, including

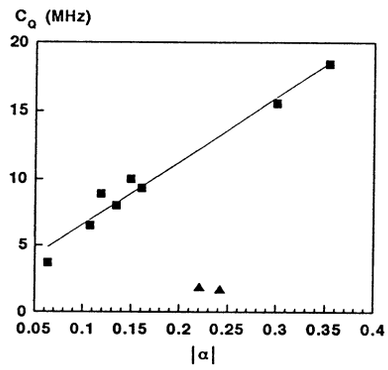

Fig. 10 Plot of C_Q (in MHz, $C_Q = e^2qQ/h$) *versus* $|a|$ (see eqn. (10). ▲: experimental data for compounds **1**, and **2**. ■: experimental data for sillimanite, kyanite, andalusite Al_2SiO_5 and zoisite $Ca_2Al_3Si_3O_{12}OH$ (see ref. 43).

data already published in the literature.[45] Obviously, our data do not fit with the correlation (established for aluminium oxide derivatives). In other words, predictions based on local distortions involving solely the first neighbours of Al atoms are absolutely not adequate for the study of derivatives **1** and **2**, which contain organic ligands. These results emphasise the fact that the electric field gradient at a quadrupolar nuclei is a quite complex physical constant and that improved calculations are needed for their correct estimation. Work is in progress for the direct calculation of C_Q for **1** and **2**. This appears as an exciting challenge as small geometrical deviations around Al atoms lead to noticeable changes in C_Q values.

Experimental

Syntheses and characterisation

Reagents and atmosphere. $AlCl_3$ (Prolabo Rectapur), $AlBr_3$ (Alfa), 85% H_3PO_4 (Prolabo Normapur), $H(C_6H_5)P(OH)O$ (Aldrich), and absolute ethanol (Prolabo Normapur) were used without further purification. The obtained crystals corresponding to compounds **1** and **2** are highly sensitive to air moisture, leading to complex amorphous derivatives upon ageing in air. Therefore, all manipulations concerning these crystals were done in a dried glove-box under an argon atmosphere. In particular, 4 mm rotors for the NMR experiments were filled with the corresponding powders in the glove-box.

$[Al_4(HPO_4)_4(C_2H_5OH)_{12}]Cl_4 \cdot 4C_2H_5OH$ (compound 1). 3.33 g (25 mmol) of anhydrous $AlCl_3$ was gently added to 50 ml of cooled ethanol (exothermic reaction). Then 2.88 g (25 mmol) of 85% H_3PO_4 was added to the solution. At 5 °C, colourless crystals are obtained after 12 hours. At RT, a white precipitate is obtained: the XRD powder pattern (transmission pattern, glass capillary (φ 0.5 mm) containing a suspension of the precipitate in the mother liquor, using an INEL diffractometer equipped with a curved detector CPS 120) is fully consistent with the crystallographic data related to compound **1**. Yield 70%. Found: C, 28.28; H, 7.14; Al, 7.90; P, 9.15; Cl, 10.37. Calc. for $C_{32}H_{100}Al_4P_4O_{32}Cl_4$: C, 28.04; H, 7.35; Al, 7.87; P, 9.04; Cl, 10.35%. ^{31}P NMR (121.44 MHz). Solid state (field 62.5 kHz, MAS 5 kHz): T_1 134 ± 4 s; $T_{1\rho}(^1H)$ 164 ± 8 ms; $T_{1\rho}(^{31}P)$ 1.44 ±

0.07 s. Solution state: EtOH: δ_P −23.6 (minor component −21.8); DMF: δ_P −3.9, −8.0, −9.5, −11.1, −14.4, −17.9; H_2O: δ_P −7.7, −11.8, −13.0, −16.9. 25 °C to 200 °C: TGA, 64 wt% loss (calc. 64.4%), DTA, endothermic: transformation into amorphous $AlPO_4$; DTA: complex weak endothermic/exothermic events, 200 °C to 400 °C; weak exothermic event, 1125 °C: crystallisation into tridymite ($AlPO_4$) (powder XRD). Heat treatment: when calcined for 5 h at 1300 °C, cristobalite ($AlPO_4$) is obtained (powder XRD).

$[Al_4(HPO_4)_4(C_2H_5OH)_{12}]Br_4 \cdot 4C_2H_5OH$ (compound 2). 6.67 g (25 mmol) of anhydrous $AlBr_3$ was gently added to 50 ml of cooled ethanol (exothermic reaction). Then 2.88 g (25 mmol) of 85% H_3PO_4 was added to the solution. At 5 °C, colourless crystals are obtained after 12 hours. Huge crystals (1 cm in one dimension) can be obtained after several days. At RT, a white precipitate is obtained: the XRD pattern is fully consistent with the crystallographic data related to compound **2**. Yield 70%. Found: Al/P/Br = 1.00/1.05/0.99. Calc. for $C_{32}H_{100}Al_4P_4O_{32}Br_4$: Al/P/Br = 1.00/1.00/1.00. C and H analyses were not reliable due to the extreme instability of the compound (several attempts were made). ^{31}P NMR (121.44 MHz). Solid state (field 62.5 kHz, MAS 5 kHz): T_1 98 ± 1 s; $T_{1\rho}(^1H)$ 45 ± 1 ms; $T_{1\rho}(^{31}P)$ 0.45 ± 0.01 s. Solution state: EtOH: δ_P −5.4, −7.4, −8.7, −13.0, −17.8, −19.5; DMF: δ_P −3.5, −5.7, −6.8, −10.8; H_2O: δ_P −5.5, −9.6, −15.0. TGA, 66.3 wt% loss (calc. 68.5%): 65% up to 400 °C, 1% up to 950 °C; DTA, 25 °C to 200°, complex endothermic events: transformation into amorphous $AlPO_4$. End of TGA–DTA: tridymite ($AlPO_4$) (powder XRD)

Analyses and spectroscopy

Elemental microanalyses. These were performed by the Centre CNRS de Vernaison, France.

Simultaneous differential thermal and thermogravimetric analyses. Analyses were performed on a TA Instrument SDT 2960 (air flow, 5 °C min^{-1}, 25 °C to 1250 °C).

Solution state NMR. Spectra were recorded on a Bruker AC 300 spectrometer (7.04 T; $\Xi^{31}P$: 121.44 MHz).

Solid state NMR. Spectra were recorded on Bruker ASX 200 (4.69 T; $\Xi^{31}P$: 80.96 MHz) and MSL 300 (7.04 T; $\Xi^{13}C$: 75.43 MHz; $\Xi^{27}Al$: 78.17 MHz; $\Xi^{31}P$: 121.44 MHz) spectrometers. Frequency of a particular nucleus is given in each Figure. Zirconia rotors were used (4 mm). Solid samples were spun at 3 to 15 kHz. Fluctuations in MAS rotation speed were smaller than ± 5 Hz over several hours. The magic angle was carefully set using the ^{79}Br resonance of KBr. Chemical shifts were referenced to $SiMe_4$ *via* solid adamantane for ^{13}C, 85% H_3PO_4 for ^{31}P and an acidic aqueous solution of $Al(NO_3)_3$ (1 M) for ^{27}Al. For ^{27}Al NMR spectra, small pulse flip angles (*i.e.* ≤ π/12) were applied, thus enabling a linear regime of excitation for the spin system.[38] Shifts in time of the FID and subsequent baseline correction were applied according to the literature.[46] $T_1(^{31}P)$ were measured by a saturation–recovery experiment (under MAS at 5 kHz). The matching of the Hartmann–Hahn (H–H) condition under moderate MAS (≤ 5 kHz) was set on adamantane (^{13}C) and compound **1** (^{31}P) (^1H 90° pulse duration: 4 μs). Typical relaxation delays were 5 to 10 s. For variable rotation speed experiments, the H–H profiles were systematically recorded. Moreover, for a given rotation speed, the H–H condition was periodically checked, especially on the MSL 300 spectrometer. The H–H matching condition was also checked by using the IRCP sequence.[36] The values of t_{CP} and t_i were set to give a null signal from the ^{31}P resonance of compound **1**: any change in $B_1(^{31}P)$ (or $B_1(^1H)$) will result in either a negative peak (improved match) or a positive peak (poorer match). This method is sensitive and proves that a slight mismatch of the H–H condition leads to erroneous line intensities using the IRCP sequence.[17b] The $T_{1\rho}(^{31}P)$ relaxation time of **1**, and **2** (at a ^{31}P spin-lock field of 62.5 kHz; MAS at 5 kHz; 7.04 T) was measured indirectly by a modified version of the CP experiment:[36] the loss of ^{31}P magnetisation was monitored as a function of the time during which the ^1H spin-lock field is turned off. The $T_{1\rho}(^1H)$ relaxation time was also measured indirectly by a modified version of the CP experiment:[36] the ^{31}P contact was established after a variable ^1H spin-lock delay. The ^{31}P CP MAS NMR spectra were recorded with 40 different contact times t_{CP} (35 experiments for ^{13}C CP MAS). The IRCP experiments were performed with 38 inversion times.

NMR experiments under fast MAS conditions (up to 14 kHz). They were performed on a Bruker ASX-200 spectrometer operating at a ^{31}P resonance frequency of 80.96 MHz and equipped with a Bruker CP/MAS probe using a 4 mm o.d. rotor. The $n = \pm 1$ Hartmann–Hahn condition was carefully matched by calibrating the ^1H and ^{31}P RF fields directly with compound **1** using a two-dimensional nutation experiment.[47] The low-power amplifier unit was employed in order to minimise any instabilities in the RF fields. Forty-four increments of contact time were recorded in the range 0–2.2 ms. Forty-eight scans were added for each experiment with a recycle time of 7 s.

Shielding tensor components as well as second-order quadrupolar lineshapes were obtained by using the WINFIT program developed by Massiot *et al.* (DM99NT version available on the web).[48] Some *Mathematica*[52] routines were used (*i.e.* numerical integration for the "fast CP MAS" experiment).

Crystallographic analysis

The selected crystals were rapidly brought out of the corresponding solutions, put in a capillary with oil and mounted on a Enraf-Nonius MACH-3 automatic diffractometer. Accurate cell dimensions (see Table 1) and orientation matrices were obtained by least-squares refinement of 25 accurately centred reflections on the diffractometer equipped with graphite-monochromated Mo-Kα radiation. Rather weak decays (≈10%) were observed in the intensities of two checked reflections during data collection; data were accordingly scaled. Computations were performed by using the PC version of CRYSTALS.[49] The data were corrected for Lorentz and polarisation effects. No correction absorption was applied. Scattering factors and corrections for anomalous absorption were taken from ref. 50. Structures were solved by direct methods (SHELXS[51]) and refined by full-matrix least squares with anisotropic thermal parameters for all non-hydrogen atoms. Hydrogen atoms were introduced in calculated positions as fixed contributors in the last refinement. The use of 1179 (for **1**) and 1347 (for **2**) reflections (with $(F_o)^2 > 3\sigma(F_o)^2$ as criterion) to refine 173 parameters led to the *R* factors listed in Table 1. Residual electronic density was −0.43 and +0.51 e $Å^{-3}$ for **1** and −0.71 and +0.69 e $Å^{-3}$ for **2**. The goodness of fit (GOF) was 1.10 for **1** and 1.04 for **2**.

CCDC reference numbers 165094 and 165095.

See http://www.rsc.org/suppdata/dt/b1/b104774b/ for crystallographic data in CIF or other electronic format.

Conclusion

In this article, we have presented the first complete solid state NMR investigations of cubane shaped aluminophosphate clusters. ^{13}C and ^{31}P CP MAS dynamics were carefully studied by variable contact time experiment or inversion recovery cross polarisation. In both cases, non-exponential growth of magnetisation was observed and explained by *coherent/incoherent* transfer of magnetisation. This is the first time that such a phenomenon has been observed in ^{31}P CP MAS NMR, and this observation should help in the understanding of spectra previously published in the literature. ^{31}P CP MAS dipolar recoupling at a high speed of rotation allowed the

direct evaluation of phosphorus–hydrogen distances in P–H and P–O–H bonds. This technique appears very powerful and of prime importance for the precise location of protons in aluminophosphate materials. Very high speed ^{31}P CP MAS (up to 33 kHz), leading to isolated spin pairs by quenching of the spin-diffusion, is now in progress. Several 1D ^{27}Al experiments converged on the precise determination of unusually low quadrupolar coupling constants. As the considered clusters are well-defined spectroscopic models, such constants could be compared to *ab initio* calculated values in a near future. Such low quadrupolar coupling constants allowed the very rare observation of multiple Solomon echoes in the time domain.

These clusters were systematically studied, as they are attractive models for cages that can be found in zeolites (typically double four-ring SBU); they can be considered as the first building block of a 3D framework. They can act as spectroscopic references for typical chemical environment in aluminophosphate related compounds.

Acknowledgements

The authors are very grateful to Mrs Jocelyne Maquet for technical assistance and helpful discussions.

References

1 S. T. Wilson, B. M. Lok, C. A. Messina, T. R. Cannan and E. M. Flanigen, *J. Am. Chem. Soc.*, 1982, **104**, 1146.
2 J. M. Bennet, W. J. Dytrych, J. J. Pluth, Jr., J. W. Richardson and J. V. Smith, *Zeolites*, 1986, **6**, 349.
3 M. E. Davis, C. Saldarriaga, C. Montes, J. Garces and C. Crowder, *Nature (London)*, 1988, **331**, 698.
4 Q. Huo, R. Xu, S. Li, Z. Ma, J. M. Thomas, R. H. Jones and A. M. Chippindale, *J. Chem. Soc., Chem. Commun.*, 1992, 875.
5 M. Estermann, L. B. McCusker, C. Maerlocher, A. Merrouche and H. Kessler, *Nature (London)*, 1991, **352**, 320.
6 (*a*) M. L. Montero, I. Uson and H. W. Roesky, *Angew. Chem., Int. Ed. Engl.*, 1994, **33**, 2103; (*b*) A. Keys, S. Bott and A. R. Barron, *Chem. Commun.*, 1996, 2339; (*c*) M. R. Mason, R. M. Matthews, M. S. Mashuta and J. F. Richardson, *Inorg. Chem.*, 1996, **35**, 5756; (*d*) M. R. Mason, M. S. Mashuta and J. F. Richardson, *Angew. Chem., Int. Ed. Engl.*, 1997, **36**, 239; (*e*) M. R. Mason, A. M. Perkins, R. M. Matthews, J. D. Fisher, M. S. Mashuta and A. Vij, *Inorg. Chem.*, 1998, **37**, 3734; (*f*) V. Chandrasekhar, R. Murugavel, A. Voigt, H. W. Roesky, H. G. Schmidt and M. Noltemeyer, *Organometallics*, 1996, **15**, 918; (*g*) C. C. Landry, A. Hynes, A. R. Barron, I. Haiduc and C. Silvestru, *Polyhedron*, 1996, **15**, 391.
7 (*a*) M. G. Walawalkar, R. Murugavel, H. W. Roesky and H. G. Schmidt, *Inorg. Chem.*, 1997, **36**, 4202; (*b*) M. L. Montero, A. Voigt, M. Teichert, I. Uson and H. W. Roesky, *Angew. Chem., Int. Ed. Engl.*, 1995, **34**, 2504; (*c*) M. G. Walawalkar, R. Murugavel, H. W. Roesky and H. G. Schmidt, *Organometallics*, 1997, **16**, 516; (*d*) K. Diemert, V. Englert, W. Kuchen and F. Sandt, *Angew. Chem., Int. Ed. Engl.*, 1997, **36**, 241; (*e*) Y. Yang, H. G. Schmidt, M. Noltemeyer, J. Pinkas and H. W. Roesky, *J. Chem. Soc., Dalton Trans.*, 1996, 3609; (*f*) D. S. Wragg, G. B. Hix and R. E. Morris, *J. Am. Chem. Soc.*, 1998, **120**, 6822; (*g*) F. J. Feher, T. A. Budzichowski and K. J. Weller, *J. Am. Chem. Soc.*, 1989, **111**, 7288.
8 Y. Yang, M. G. Walawalkar, J. Pinkas, H. W. Roesky and H. G. Schmidt, *Angew. Chem., Int. Ed.*, 1998, **37**, 96.
9 Q. Gao, R. Xu, J. Chen, S. Li, S. Qiu and Y. Yue, *J. Chem. Soc., Dalton Trans.*, 1996, 3303.
10 B. T. Holland, P. K. Isbester, C. F. Blanford, E. J. Munson and A. Stein, *J. Am. Chem. Soc.*, 1997, **119**, 6796.
11 M. G. Voronkov and V. I. Lavrent'yev, *Top. Curr. Chem.*, 1982, **102**, 199.
12 (*a*) M. Backer, A. R. Grimmer, N. Auner, P. Jahn and J. Weis, *Solid State Nucl. Magn. Reson.*, 1997, **9**, 241; (*b*) C. Bonhomme, P. Toledano, J. Maquet, J. Livage and L. Bonhomme-Coury, *J. Chem. Soc., Dalton Trans.*, 1997, 1617.
13 J. E. Cassidy, J. A. J. Jarvis and R. N. Rothon, *J. Chem. Soc., Dalton Trans.*, 1975, 1497.
14 T. Gullion and J. Schaefer, *J. Magn. Reson.*, 1989, **81**, 196.
15 A. W. Hing, S. Vega and J. Schaefer, *J. Magn. Reson.*, 1992, **96**, 205.
16 (*a*) A. Pines, M. G. Gibby and J. S. Waugh, *J. Chem. Phys.*, 1973, **59**, 569; (*b*) M. Mehring, in *Principles of High Resolution NMR in Solids*, Springer, Berlin, 1983, pp. 151–168.
17 (*a*) X. Wu, S. Zhang and X. Wu, *Phys. Rev. B*, 1988, **37**, 9827; (*b*) X. Wu and K. W. Zilm, *J. Magn. Reson., Ser. A*, 1993, **102**, 205.
18 (*a*) P. Palmas, P. Tekely and D. Canet, *J. Magn. Reson., Ser. A*, 1993, **104**, 26; (*b*) J. Hirschinger and M. Hervé, *Solid State Nucl. Magn. Reson.*, 1994, **3**, 121.
19 R. Sangill, N. Rastrup-Andersen, H. Bildsoe, H. J. Jakobsen and N. C. Nielsen, *J. Magn. Reson., Ser, A*, 1994, **107**, 67.
20 (*a*) P. Tekely, V. Gérardy, P. Palmas, D. Canet and A. Retournard, *Solid State Nucl. Magn. Reson.*, 1995, **4**, 361; (*b*) P. Reinheimer, J. Hirschinger, P. Gilard and N. Goetz, *Magn. Reson. Chem.*, 1997, **35**, 757.
21 (*a*) S. Ding, C. A. McDowell and C. Ye, *J. Magn. Reson., Ser. A*, 1994, **109**, 1; (*b*) S. Ding, C. A. McDowell and C. Ye, *J. Magn. Reson., Ser. A*, 1994, **109**, 6.
22 W. P. Rothwell, J. S. Waugh and J. P. Yesinowski, *J. Am. Chem. Soc.*, 1980, **102**, 2637.
23 G. L. Turner, K. A. Smith, R. J. Kirkpatrick and E. Oldfield, *J. Magn. Reson.*, 1986, **70**, 408.
24 (*a*) T. Blasco, J. Pérez-Pariente and W. Kolodziejski, *Solid State Nucl. Magn. Reson.*, 1997, **8**, 185; (*b*) W. Kolodziejski and J. Klinowski, *J. Phys. Chem. B*, 1997, **101**, 3937; (*c*) A. Kaflak, D. Chmielewski, A. Gorecki and W. Kolodziejski, *Solid State Nucl. Magn. Reson.*, 1998, **10**, 191.
25 F. Taulelle, A. Samoson, T. Loiseau and G. Férey, *J. Phys. Chem. B*, 1998, **102**, 8588.
26 E. W. Hagaman, P. C. Ho, L. L. Brown, F. M. Schell and M. C. Woody, *J. Am. Chem. Soc.*, 1990, **112**, 7445.
27 P. Bertani, J. Raya, P. Reinheimer, R. Gougeon, L. Delmotte and J. Hirschinger, *Solid State Nucl. Magn. Reson.*, 1999, **13**, 219.
28 P. Bertani, Ph. D. Thesis, Université Louis Pasteur, Strasbourg, France, September, 2001, p. 103.
29 L. Müller, A. Kumar, T. Baumann and R. Ernst, *Phys. Rev.Lett.*, 1974, **32**, 1402.
30 B. H. Meier, *Chem. Phys. Lett.*, 1992, **188**, 201.
31 X. Wu and K. W. Zilm, *J. Magn. Reson., Ser. A*, 1993, **104**, 154.
32 (*a*) T. G. Oas, R. G. Griffin and M. H. Levitt, *J. Chem. Phys.*, 1988, **89**, 692; (*b*) N. C. Nielsen, H. Bildsoe, H. J. Jakobsen and M. H. Levitt, *J. Chem. Phys.*, 1994, **101**, 1805.
33 (*a*) N. A. Curry and D. W. Jones, *J. Chem. Soc. A*, 1971, 3725; (*b*) M. Catti and G. Ivaldi, *Z. Kristallogr.*, 1977, **146**, 215; (*c*) M. Catti, G. Ferraris and A. Filhol, *Acta Crystallogr., Sect. B*, 1977, **33**, 1223; (*d*) A. M. Krogh Andersen, P. Norby, J. C. Hanson and T. Vogt, *Inorg. Chem.*, 1998, **37**, 876.
34 *International Tables for X-ray Crystallography*, Kynoch Press, Birmingham, 1968, vol. III, pp. 265.
35 M. T. Melchior, Proceedings of the 22nd Experimental NMR Conference, Asilomar, 1981; (poster B29).
36 L. W. Jelinski and M. T. Melchior, in *NMR Spectroscopy Techniques*, Marcel Dekker, Inc.,New York, 1987, pp. 253–329.
37 A. Samoson and E. Lippmaa, *J. Magn. Reson.*, 1988, **79**, 255.
38 (*a*) P. P. Man, *Mol. Phys.*, 1993, **78**, 307; (*b*) P. P. Man, E. Duprey, J. Fraissard, P. Tougne and J.-B. d'Espinose, *Solid State Nucl. Magn. Reson.*, 1995, **5**, 181.
39 I. Solomon, *Phys. Rev.*, 1958, **110**, 61.
40 P. P. Man, *J. Chem. Phys.*, 1997, **106**, 3908.
41 I. D. Weisman and L. H. Bennet, *Phys. Rev.*, 1969, **181**, 1341.
42 A. Samoson, *Chem. Phys. Lett.*, 1985, **119**, 29.
43 J. Skibsted, P. Norby, H. Bildsoe and H. J. Jakobsen, *Solid State Nucl. Magn. Reson.*, 1995, **5**, 239.
44 D. Massiot, D. Müller, T. Hübert, M. Schneider, A. P. M. Kentgens, B. Coté, J.-P. Coutures and W. Gessner, *Solid State Nucl. Magn. Reson.*, 1995, **5**, 175.
45 (*a*) S. Ghose and T. Tsang, *Am. Miner.*, 1973, **58**, 748; (*b*) S. S. Hafner, M. Raymond and S. Ghose, *J. Chim. Phys.*, 1970, **52**, 6037.
46 F. Taulelle, C. Bessada and D. Massiot, *J. Chem. Phys.*, 1992, **89**, 379.
47 A. Bax, in *Two-Dimensional NMR in Liquids*, Delft University Press, Delft, 1984.
48 D. Massiot, H. Thiele and A. Germanus, Bruker Report, 1994, **140**, p. 43.
49 D. J. Watkin, C. K. Prout, J. R. Carruthers and P. W. Betteridge, in *Crystal Issue 10*, Chemical Crystallography Laboratory, University of Oxford, UK, 1996.
50 D. T. Cromer, in *International Tables for X-ray Crystallography*, Kynoch Press, Birmingham, 1974, vol. IV.
51 G. M. Sheldrick, SHELXS86, Program for the Solution of Crystal Structures, University of Göttingen, Germany, 1986.
52 S. Wolfram, *The Mathematica Book*, Wolfram Media/Cambridge University Press, 1999.